ACS OMEGA

http://pubs.acs.org/journal/acsodf

Article

Properties and Corrosion Resistance Mechanism of a Self-Healing Propane−1,2,3-Triol-Loaded Polysulfone Microcapsule Coating Loaded with Epoxy Resin

Qingping Zhao, Shumei Kang,* Fangzheng Zou, Zhongbo Zhu, Jian Kang, and Yansheng Yin

Cite This: *ACS Omega* 2022, 7, 21868−21876

Read Online

ACCESS | Metrics & More | Article Recommendations | Supporting Information

ABSTRACT: Propane−1,2,3-triol-loaded polysulfone (PSF) microcapsules were prepared by the solvent evaporation method. The particle size of the microcapsules is about 140 μm. The shell wall thickness is about 17 μm approximately. The microcapsules have high thermal stability and antiwear performance. The self-healing coating was prepared by adding the prepared capsule into the epoxy resin coating. After electrochemical and corrosion immersion experiments, the resistance modulus of the coating added to the microcapsules was higher than the others in a 3.5 wt % NaCl corrosion solution, and it had the lowest corrosion current density, so the self-healing microcapsule coatings showed excellent healing ability and corrosion inhibition function for microcracks. This was attributed to the formation of a hydrophobic film after propane−1,2,3-triol was released from the damaged microcapsules.

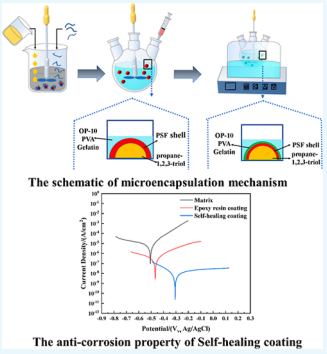

1. INTRODUCTION

Many coatings with different functions are used to improve the properties of metal materials,[1−3] such as superhydrophobic coating,[4,5] antibacterial coating,[6,7] heat-insulating coating,[8,9] and self-healing coating.[10,11] In particular, self-healing coatings have attracted much attention because they can produce a secondary healing effect, which can delay the corrosion process and provide long-lasting corrosion resistance. Most self-healing coatings use the microcapsule shell as a carrier to encapsulate the corrosion inhibitor. When the coating is damaged by stress, the corrosion inhibitor is released to delay the corrosion process.[12,13] Various corrosion inhibitors are embedded in microcapsules and mixed with polymers to produce self-healing coatings.[14,15] It has been reported that corrosion inhibitors, including linseed oil (LO),[16−19] tung oil (TO),[20−22] seed oil (SO),[23−25] and soybean oil (CCO),[26] have been successfully microencapsulated. Researchers added them to the polymer to prepare a self-healing corrosive coating.

da Cunha et al.[27] studied the dual-functional poly(urea formaldehyde) microcapsules, and they were used with linseed oil and benzotriazole (BTA). Li et al.[28] encapsulated tung oil into polysulfone successfully. Li[29] studied that self-healing microcapsules were prepared by the solvent evaporation method with polysulfone (PSF) as the shell and tung oil as core materials because PSF has relatively stable chemical properties and high thermal stability. It has been widely used in the coating of self-healing microcapsules with lubricating function.[30−32]

The corrosion resistance and protection efficiency of PSF microcapsule self-healing coating need further study. It is particularly important to analyze the corrosion resistance of the self-healing PSF microcapsule coating by electrochemical methods. In this work, a protective film was prepared by the combination of propane−1,2,3-triol and PSF.

2. EXPERIMENTAL SECTION

2.1. Materials. Epoxy resin was obtained from Guangzhou Lihou Trading Co, Ltd. Propane−1,2,3-triol (99.5%) was obtained from Shanghai Bide Pharm Technology Co. Gelatin, tetraethylenepentamine (TEPA), ethanol, and the emulsifier OP-10 were purchased from Tianjin Aopusheng Chemical Co. PSF was bought from Shanghai Macklin Biochemical Co, Ltd. Polyvinyl alcohol (PVA) (wt 30 000−70 000) was provided by Sigma-Aldrich Trading Co. Ltd. Dichloromethane (>99.5%) was obtained from Liaoning Quanrui Reagent Co, Ltd. All chemicals were used directly without further treatment.

2.2. Preparation of Propane−1,2,3-Triol-Loaded Microcapsules. PSF microcapsules containing propane−1,2,3-triol were obtained by the solvent evaporation method. 1 g of PSF was dissolved in 20 mL of methylene chloride. Then, 1.2 mL of propane−1,2,3-triol was added to the mixture of PSF and methylene chloride. Then, the previous solutions were added to 50 mL of a mixture of 0.8 wt % PVA and 1 wt % gelatin as slowly as possible, which were mechanically emulsified at 800 rpm and

Received: April 1, 2022
Accepted: June 2, 2022
Published: June 13, 2022

https://doi.org/10.1021/acsomega.2c02026
ACS Omega 2022, 7, 21868−21876

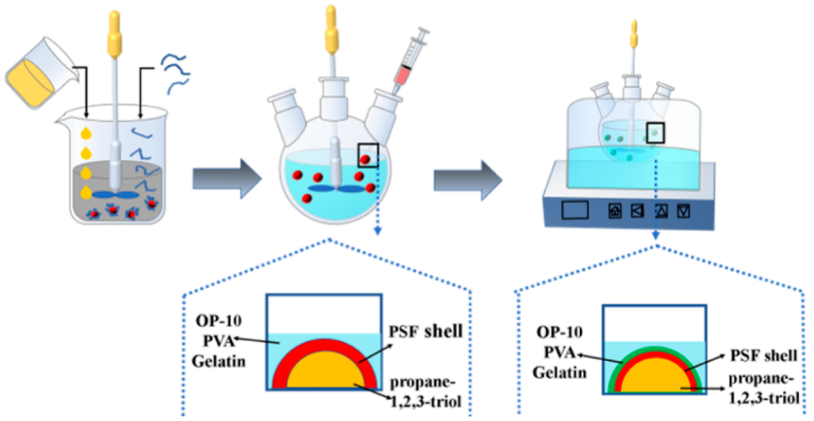

Figure 1. Schematic of the microencapsulation mechanism.

reacted at 38 °C for 4 h until methylene chloride was completely evaporated. After the reaction, the propane−1,2,3-triol-loaded PSF microcapsules were separated by filtering and washing them with deionized water. Finally, the propane−1,2,3-triol-loaded PSF microcapsules were dried in a drying vacuum oven at 50 °C. The preparation mechanism is shown in Figure 1.

2.3. Preparation of Composite Coating. Self-healing epoxy resin coatings were obtained by mixing the epoxy resin and TEPA curing agent. Then, the prepared microcapsules were added part by part to the epoxy resin with stirring for 30 min. Steel panels (30 mm × 30 mm × 1.5 mm) were polished with a 1500 grade waterproof abrasive paper and then washed with acetone in an ultrasonic bath, whereafter 30% TEPA was added into the previously prepared mixture. The epoxy resin mixture was stirred for 30 min. Then, the evenly mixed epoxy resin mixture was neatly covered on the sample work surface. Finally, the coatings were cured at 25 °C for 4 h and 80 °C for 6 h in the drying oven.

3. CHARACTERIZATIONS OF MICROCAPSULES

3.1. Chemical Composition Analysis. The chemical components of propane−1,2,3-triol, PSF, and propane−1,2,3-triol-loaded PSF microcapsules were characterized by Fourier transform infrared (FTIR) spectroscopy with the wavelength range from 4000 to 450 cm^{-1}.

3.2. Morphology of Coatings and Microcapsules. The internal and external morphology of propane−1,2,3-triol-loaded PSF microcapsules was observed by scanning electron microscopy (SEM). In order to obtain the best observation, all of the microcapsules were coated with a layer of gold. Also, the cross-sections of coatings were coated with a layer of gold. The thickness of the core−shell, size of microcapsules, and cross-section of coatings were observed by SEM.

3.3. Thermal Stability. The thermal stabilities of propane−1,2,3-triol, PSF, and propane−1,2,3-triol-loaded PSF microcapsules were analyzed by thermal gravimetric analysis (TGA) under the protection of nitrogen (N_2), ranging from 30 to 600 °C, at a heating rate of 10 °C/min.

3.4. Core Fraction and Microencapsulation Efficiency. The dried microcapsules were weighed as M_1. Then, the dried microcapsules were mashed using a porcelain mortar and thoroughly soaked in acetone. M_2 is the weight of the shell material which was centrifuged and dried. M is the weight of propane−1,2,3-triol added. the encapsulation efficiency can be calculated by eq 1. R is the encapsulation efficiency.

$$R = \frac{M_1 - M_2}{M} \times 100\% \quad (1)$$

3.5. Evaluation of the Self-Healing Epoxy Resin Coating. The coating with microcapsules and the epoxy resin coating without microcapsules were cross-scratched using a knife. Then, the scratched coatings were immersed in a corrosion solution (10 wt % NaCl solution) for 1−7 d.[29] A camera was used to observe the corrosion state of the coating at different times.

3.6. EIS Measurements. Electrochemical impedance experiments have been performed with an electrochemical workstation using a one-compartment three-electrode cell. The corrosion solution is artificial seawater, which is a naturally aerated 3.5% NaCl solution prepared by mixing ultrapure water with NaCl. The working electrode, reference electrode, and auxiliary electrode were the coated or uncoated specimens, Ag/AgCl electrode, and platinum sheet, respectively. Open-circuit potential (OCP) versus time prior to electrochemical impedance spectroscopy (EIS) is necessary to maintain the stability of the OCP data. EIS was carried out with an amplitude of 10 mV, using the typical frequency test range from 10^{-2} to 10^5 Hz. Potentiodynamic polarization curves were measured at a scan rate of 1 mV/s. The obtained data were analyzed with the help of the fit function of the Zview software.

3.7. Evaluation of Mechanical Properties. The mechanical properties of epoxy resin coating coatings and self-healing epoxy resin coating were studied by using a dowel-type friction wear test machine (as shown in the schematic diagram in Figure 2). The pressure was 1.0 MPa, and the sliding speed was 0.51 m/s. The pinheads of all texts were treated with 1000 mesh

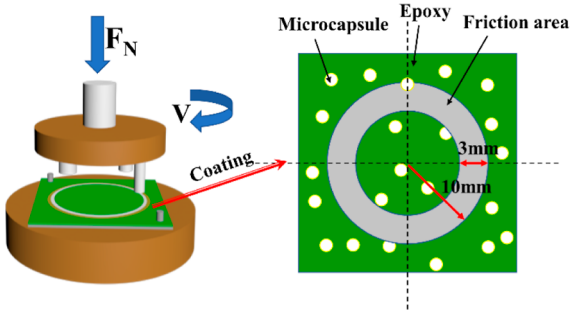

Figure 2. Schematic diagram for friction and wear tests.

https://doi.org/10.1021/acsomega.2c02026
ACS Omega 2022, 7, 21868−21876

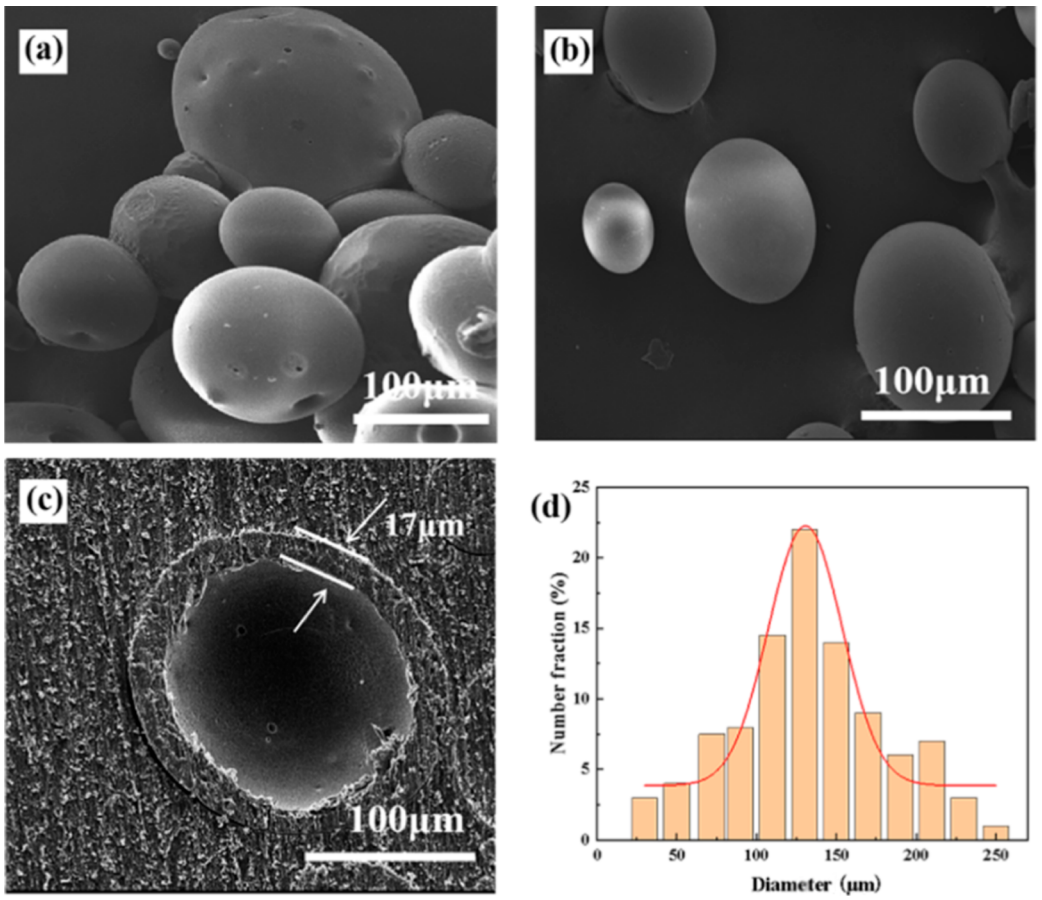

Figure 3. SEM images and size distribution of propane−1,2,3-triol-loaded microcapsules: (a) microcapsule magnification: 200×, (b) microcapsules magnification: 500×, (c) ruptured microcapsule: 500×, and (d) size distribution.

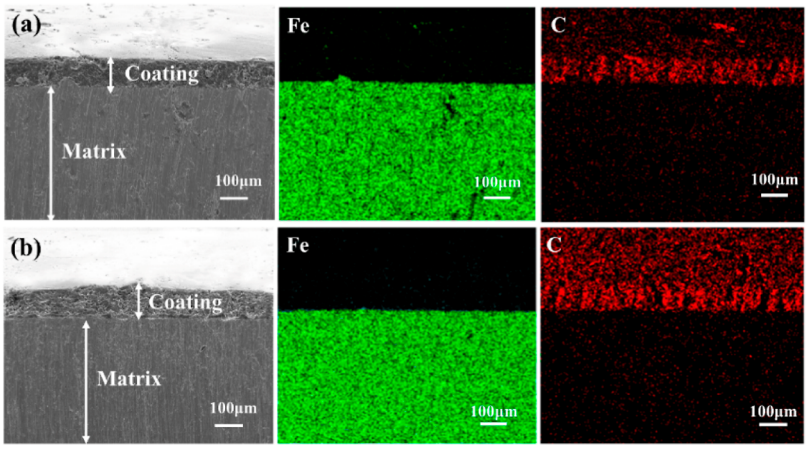

Figure 4. Cross-sectional SEM and EDS element mapping images: (a) epoxy resin coating and (b) self-healing coating.

sandpaper and then cleaned with ethanol prior to the friction test.

4. RESULTS AND DISCUSSION

4.1. Morphology of Microcapsules and Coatings. Figure 3a shows the SEM images of propane−1,2,3-triol-loaded microcapsules. Figure 3b shows the SEM images of a single microcapsule. The synthetic capsule is spherical with a smooth surface. The capsules form a compact distribution of structures. The shell wall thickness of the microcapsule is about 16 μm as observed in the SEM images in Figure 3c. Figure 3d shows the particle-size distribution of the microcapsules, and the average diameter of the particles was approximately 140 μm.

To study the epoxy resin coating and self-healing coating morphology, the two coating cross-sections were investigated using field-emission SEM and energy-dispersive system (EDS) mapping. Figure 4 shows the SEM images and elemental mapping of the epoxy resin coating and self-healing coating cross-sections. For elemental mapping, carbon (C) is the main constituent of the epoxy resin coating and self-healing coating. Iron (Fe) is the main constituent of the matrix. Carbon (C) and iron (Fe) were selected as the elements to be measured. Figure

https://doi.org/10.1021/acsomega.2c02026
ACS Omega 2022, 7, 21868−21876

4a shows the SEM image and elemental mapping of the epoxy resin coating. Figure 4b shows the cross-sectional imaging and elemental analysis of the self-healing coating. As shown in Figure 4, the film thickness of epoxy resin coating and self-healing coating is in the range of 90−95 μm. Both coatings are tightly bound to the matrix, but the addition of microcapsules makes the coating denser.

4.2. Chemical Structure Analysis of Microcapsules. FTIR spectroscopy was used to determine whether propane−1,2,3-triol was encapsulated in the microcapsule. The FTIR spectra of microcapsules and propane−1,2,3-triol and PSF are presented in Figure 5. As shown in Figure 4, the characteristic peak of propane−1,2,3-triol are shown at 3288 cm^{-1} (−OH stretching vibration), 2931 cm^{-1} (asymmetric stretching vibration of $-CH_2$), 2878 cm^{-1} (symmetric stretching vibration of $-CH_2$), 1413 cm^{-1} (bending vibration peak of $-CH_2$), 1030 and 992 cm^{-1} (the symmetric stretching vibration of C−O), and 1108 cm^{-1} (the symmetric stretching vibration peak of C−O of secondary alcohol). The characteristic peaks of PSF are at 1488− and 1587 cm^{-1} (C−C aromatic ring stretching vibration), 1322 and 1294 cm^{-1} (O−S−O asymmetric stretching vibration), and 1239 cm^{-1} (C−O−C stretching vibration).[30] The peaks of the microcapsules occurred at 2979 and 2901 cm^{-1}. The characteristic peaks of propane−1,2,3-triol and PSF were reflected in the characteristic peaks of the microcapsules, which confirmed that propane−1,2,3-triol was successfully coated with PSF.

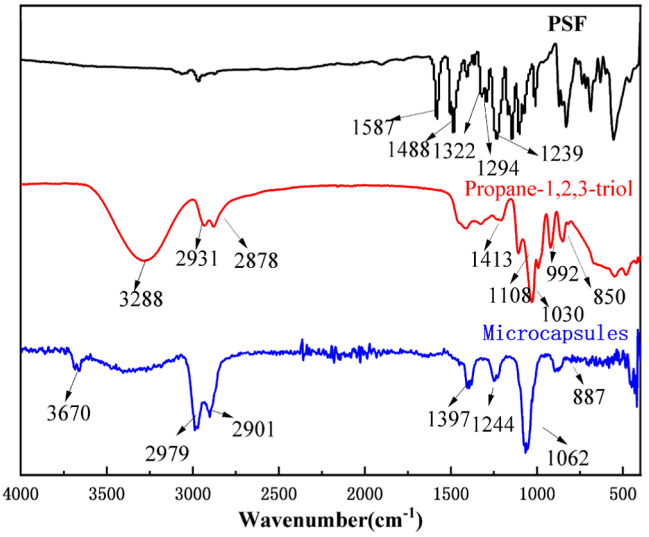

Figure 5. FTIR spectra of microcapsules, propane−1,2,3-triol, and PSF.

4.3. TGA and Microencapsulation Efficiency. For comparison, the TGA curve of microcapsules is also shown. Figure 6 shows that the initial decomposition temperature of PSF was 450 °C. The initial decomposition temperature of PSF is higher than polyurethane foam (PUF), polyurea, and poly(melamine formaldehyde). The amount of residue was 31 wt % at 800 °C. It presumably formed the heat-stabilized material for carbon. Because the PSF polymer has the presence of an aromatic structure backbone. Pure propane−1,2,3-triol has an initial decomposition temperature of 150 °C. Its end decomposition temperature is 278 °C. The initial temperature of thermal degradation of microcapsules was 320 °C. The slope of this curve was less than the PSF. This indicates that propane−1,2,3-triol was successfully encapsulated by PSF. TGA identified that both of the pure propane−1,2,3-triol core and PSF shell constituted the synthesized microcapsules. According to the TGA curve of the microcapsules, the encapsulation capacity of the microcapsules was 12 wt %. The results are consistent with those obtained by acetone extraction.

4.4. Antiwear Performance of Self-Healing Coatings. The tribological tests of three samples were carried out under 1 MPa at 0.51 m/s. Figure 7 shows the coefficient of friction of the

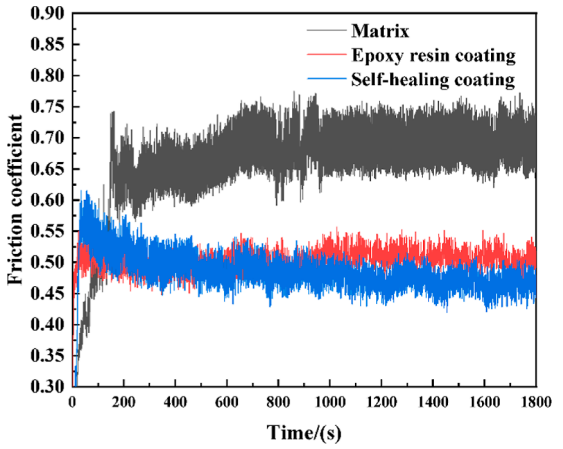

Figure 7. Frictional coefficient of the matrix, epoxy resin coating, and self-healing coating.

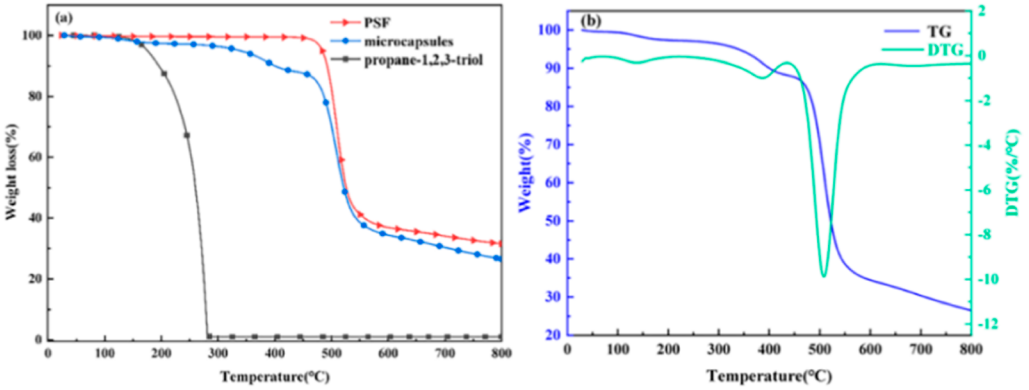

Figure 6. Thermal stability analysis: (a) TGA curves of PSF, propane−1,2,3-triol-filled microcapsules, and propane−1,2,3-triol. (b) DTG curve of microcapsules.

https://doi.org/10.1021/acsomega.2c02026
ACS Omega 2022, 7, 21868−21876

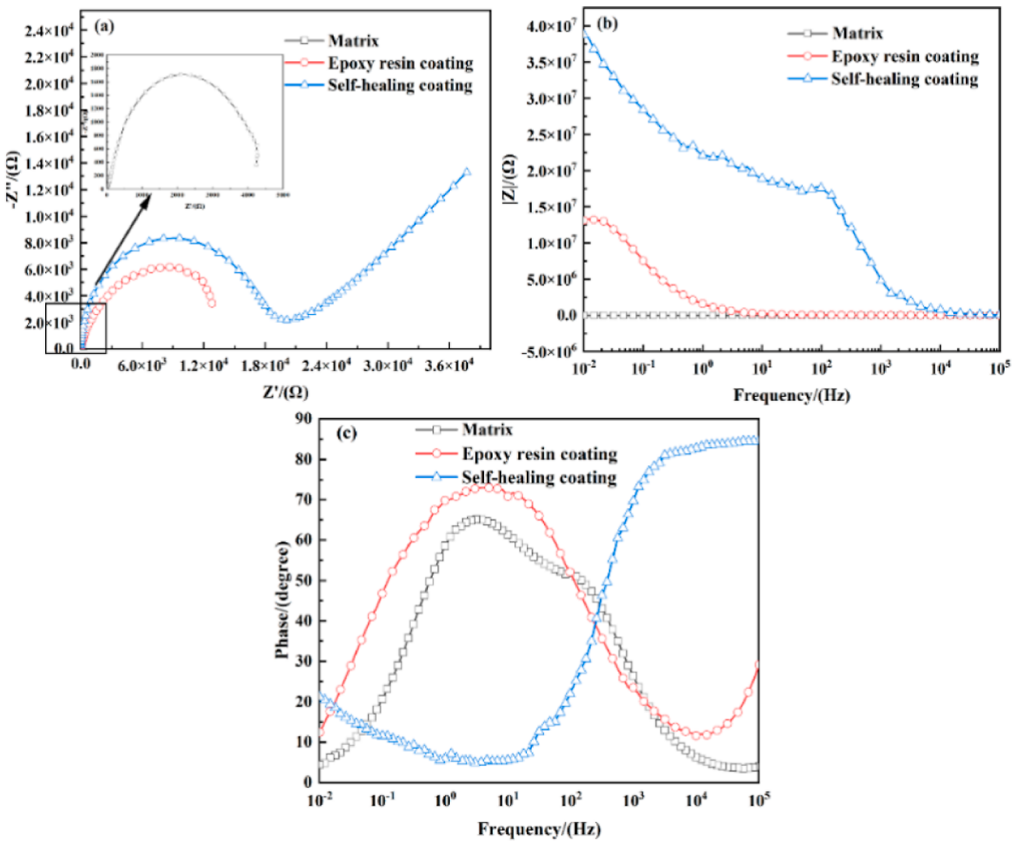

Figure 8. Nyquist and Bode plot of uncoated AH36, epoxy resin coating, and self-healing epoxy resin coating in the 3.5% NaCl solution: (a) Nyquist plot, (b) impedance mode vs frequency plot, and (c) phase angle vs frequency plot.

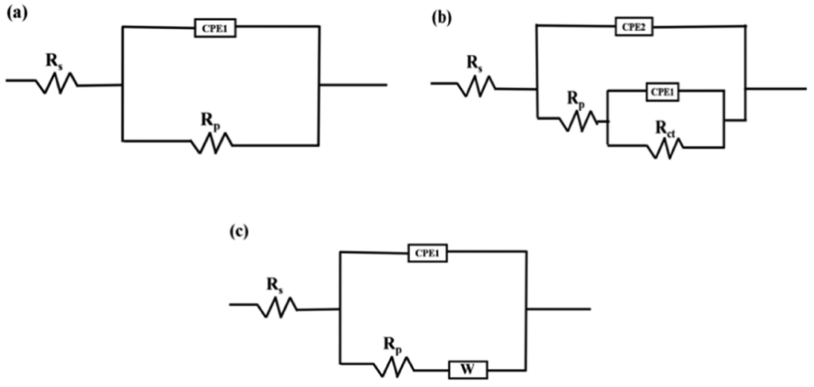

Figure 9. EIS equivalent simulation circuit diagram: (a) for the uncoated matrix, (b) for the epoxy resin coating, and (c) for the self-healing epoxy resin coating.

epoxy resin coating and self-healing coating. With the addition of microcapsules, it can be seen that the friction coefficients decrease sharply at first. The friction coefficient of the matrix is 0.65. The friction coefficient of the coating with microcapsules is 0.48 and that without microcapsules is 0.50. This may be related to the self-lubrication action of the newly formed propane−1,2,3-triol film between the epoxy resin and sliding surface. Propane−1,2,3-triol was extruded from the broken microcapsules under the friction. Moreover, the wear debris of PSF shells can compound propane−1,2,3-triol as a solid lubricant. Propane−1,2,3-triol and PSF shells improved the wear resistance of the epoxy resin coatings.

4.5. Corrosion Performance of Self-Healing Coatings. To assess the corrosion resistance of different kinds of samples, we performed EIS measurements. Impedance spectra represented in both complex impedance diagrams (Nyquist plot) and the Bode plot are illustrated in Figure 7.

Figure 8a,b shows that the impedance modulus values of the matrix and the two coatings (three samples) in the low-frequency region are 4.2×10^3, 1.3×10^7, and 3.8×10^7 Ω/cm^2, respectively. With the larger diameter of the semicircle in the corrosion solution, the charge-transfer resistance is larger together with excellent corrosion resistance. Thus, the order of corrosion resistance of samples is self-healing epoxy resin coating > epoxy resin film > matrix. Figure 8b shows the impedance mode versus frequency plot of epoxy resin coating. The dot product of the impedance magnitude at 0.01 Hz is above 10^7. The results show that the epoxy coating can

https://doi.org/10.1021/acsomega.2c02026
ACS Omega 2022, 7, 21868−21876

Table 1. Electrochemical Impedance Parameters

coatings	CPE1 [μF cm^{-2}]	R_c [Ω/cm^2]	CPE2 [μF cm^{-2}]	R_{ct} [Ω/cm^2]	W
blank	1.09×10^{-4}			6.529×10^3	
epoxy resin coating	1.39×10^{-7}	1.29×10^5	5.02×10^{-9}	1.55×10^7	
self-healing coating		1.53×10^7	3.61×10^{-11}		1.99×10^7

effectively isolate the contact between the electrolyte solution and matrix. It also can provide good corrosion resistance for the matrix. In Figure 8a, it can be seen that the Nyquist plot of the self-healing epoxy resin coating consists of capacitive arcs and a diffusion tail. Besides, in the Bode plot, the impedance magnitude of the self-healing epoxy resin coating is 3 times that of the epoxy resin coating. This indicates that the self-healing microcapsule improves the stability of the coating. Also, the self-healing microcapsule enhanced the physical function of the coating to block corrosive ions. The long diffusion tail in the low-frequency region is due to the rupture of the microcapsule, which leads to the increase of the surface roughness of the coating. In addition, the corrosion inhibitor is released to the corrosion site, forming an adsorption film and improving the corrosion resistance of the coating.

The EIS data were fitted by using the matching equivalent circuit models for further analysis (Figure 9). The parameters obtained by fitting are listed in Table1. R_s, R_c, R_{ct}, CPE, and W represent the solution resistance, coating resistance, charge-transfer resistance, constant phase element, and Warburg resistance, respectively.

The solution resistance R_s between 2 and 10 Ω/cm^2 can be ignored. Coating resistance (R_c) reflects the blocking ability of the electrolyte solution through the coating. It is essential to assess the corrosion resistance of coatings in detail. The CPE is related to the diffusion behavior of the electrolyte solution in the coating. The permittivity of the coating changes when the electrolyte solution penetrates the coating. The CPE changes. Therefore, the CPE reflects the penetration resistance of the coating. Figure 9a−c shows the equivalent circuit models of the electrochemical impedance behavior of the matrix, epoxy resin coating, and self-healing epoxy resin coating, respectively. Figure 8c shows a time constant in the phase angle versus frequency plot of the matrix, which is fitted by the equivalent circuit models shown in Figure 9a. The charge-transfer resistance of the matrix is 6.5×10^3 Ω/cm^2, and the capacitance of the matrix is 1.09×10^{-4} μF/cm^2. The matrix shows general corrosion in the electrolyte solution. The phase angle versus frequency plot of the epoxy resin coating in Figure 8c generates two time constants, which are fitted using the equivalent circuit models shown in Figure 9b. The Nyquist plot of the self-healing epoxy resin coating consists of a capacitive arc and long diffusion tail. Also, there is a time constant in Figure 8c. The equivalent circuit model as shown in Figure 9c was used for fitting. As shown in Table 1, the charge-transfer resistance of the matrix is 6.529×10^3 Ω/cm^2 and that of the epoxy resin coating is 1.55×10^7 Ω/cm^2. The charge-transfer resistance of the epoxy coating is 4 times larger than that of the matrix. It shows that the reaction resistance of the substrate surface is small, and the corrosion degree is serious. The epoxy resin coating on the surface of the matrix significantly increases the corrosion resistance. The coating resistance (R_c) of the self-healing epoxy resin coating is 2 times dot product larger than that of the epoxy resin coating. The self-healing epoxy resin coating successfully resists the penetration of the electrolyte solution into the matrix and coating surface. The microcapsule releases the corrosion inhibitor to adsorb on the corrosion site. It inhibits the corrosion process successfully.

Figure 10 shows the polarization curves of the matrix, epoxy resin coating, and self-healing coating in the 3.5 wt % NaCl solution at room temperature. Details of the polarization curves calculated by Tafel extrapolation are shown in Table 2. CR and PE are the annual corrosion rate and anticorrosion efficiency, respectively, in the Tafel curve.

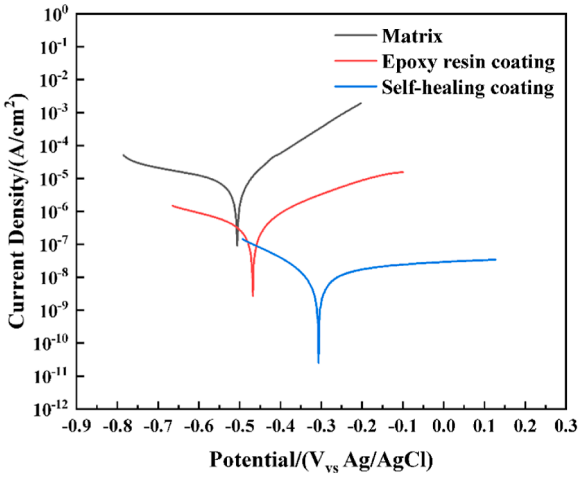

Figure 10. Tafel plots of the matrix, epoxy resin coating, and self-healing coating immersed in the 3.5 wt % NaCl solution.

Table 2. Electrochemical Parameters of the Uncoated and Coated Matrix

coatings	E_{corr} [V]	I_{corr} [A/cm^2]	CR [mm/a]	PE [%]
blank	−0.508	6.37×10^{-6}	1.48×10^{-1}	
epoxy resin coating	−0.472	2.97×10^{-7}	6.91×10^{-3}	95.65
self-healing coating	−0.303	8.32×10^{-9}	1.94×10^{-4}	99.87

The CR and PE were obtained by the following eqs 2 and 3, respectively

$$\mathrm{CR} = \frac{KM_m I_{corr}}{\rho_m} \quad (2)$$

where CR represents the annual corrosion rate. I_{corr} represents the corrosion current density in the absence and presence of coatings for the bare matrix, and K, M_m, and ρ_m represent the constant, relative atomic mass, and density, respectively.

$$\mathrm{PE} = \frac{I_{corr,o} - I_{corr,i}}{I_{corr,o}} \times 100\% \quad (3)$$

where PE represents the protection efficiency. $I_{corr,o}$ and $I_{corr,i}$ represent the corrosion current density in the absence and presence of coatings for the bare matrix, respectively.

E_{corr} mainly describes the trend of corrosion thermodynamics of coatings rather than a standard for assessing the corrosion

https://doi.org/10.1021/acsomega.2c02026
ACS Omega 2022, 7, 21868−21876

resistance of coatings. Generally speaking, the corrosion resistance is mainly judged by the corrosion current density. The lower current density shows the lower corrosion rate. Compared to the matrix, the epoxy resin coating and self-healing coating have lower orders of magnitude of current density. These results indicate that the two coatings can effectively slow down the corrosion rate and provide excellent protection for the matrix obviously. Furthermore, self-healing coatings work better in a NaCl solution. The reason is that the coating successfully resists the penetration of electrolyte solution into the matrix and coating surface. The microcapsule releases the corrosion inhibitor to adsorb on the corrosion site. It inhibits the corrosion process successfully.

4.6. Self-Healing Mechanism. Figure 11 shows the visual appearance of the scratched area of the coated sample after 7 d.

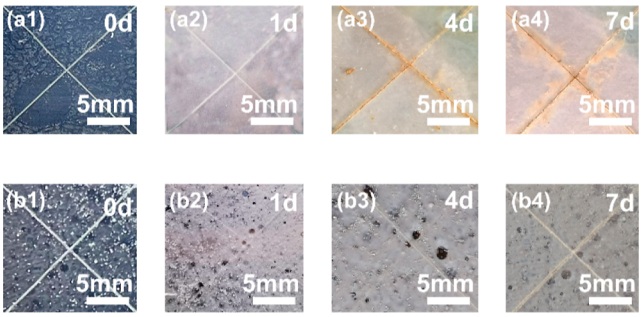

Figure 11. Immersion study performance: (a) epoxy resin coating and (b) self-healing coating.

For the neat epoxy resin, rusting occurred along the scratched area. The longer the immersion time, the more serious the corrosion. The steel plate coated with the self-healing coating was not corroded in the scratched area after 1 d. The self-healing coating has strong corrosion resistance because the microcapsule has the corrosion inhibitor.

As shown in Figure 12, propane−1,2,3-triol in the microcapsule is released when the epoxy resin coating is damaged. Because of this, the substrate surface rapidly forms a protective film. It can slow down the hydrogen ions, chlorine ions, and water molecules from entering the matrix in the solution, thus reducing corrosion and the corrosion rate. In this way, the corrosion of the metal is delayed. Propane−1,2,3-triol is a polar molecule. The unshared electron pair of oxygen elements on polar substrates and the hydrogen ion-bonded. It can result in cation adsorption on the surface of the matrix. Finally, it changed the structure of the electric double layer on the surface of the matrix. The activation energy of the carbon steel ionization process increased. However, nonpolar groups made directional arrangement away from the metal surfaces. It forms a layer of a hydrophobic membrane to produce the cover effect. When chloride ions are present in the solution, the substrate surface has a positive charge. Thus, the chloride ions can remain painlessly on the surface. The zero-charge potential is moved in the right direction, thus inhibiting the anode reaction. The surface adsorption of chloride ions contributes to the formation of the propane−1,2,3-triol cation adsorption layer. It not only increases the activation energy of the corrosion reaction but also impedes the charge transfer. It also generates anodic polarization and reduces corrosion. Therefore, this anionic effect weakens corrosion.

5. CONCLUSIONS

Based on the preparation of PSF microcapsules containing the propane−1,2,3-triol corrosion inhibitor in a micron container, PSF has relatively stable chemical properties and high thermal stability, and propane−1,2,3-triol and hydrogen ions can form a hydrophobic film on the metal surface. It can slow down the hydrogen ions, chlorine ions, and water molecules from entering the matrix in the solution, thus reducing corrosion and the corrosion rate.

1. The microcapsule containing the corrosion inhibitor was coated in an epoxy coating to form a self-healing coating microcapsule with a smooth spherical geometric surface.
2. The particle size of the propane−1,2,3-triol-loaded PSF microcapsules is 140 μm.
3. TGA and FTIR test results showed that the corrosion inhibitor was effectively wrapped in the PSF shell. The DTG curve of microcapsules showed that the PSF shell was loaded with about 12 wt % inhibitor.
4. The cross-sectional SEM image showed that the addition of microcapsules makes the coating dense. Also, the

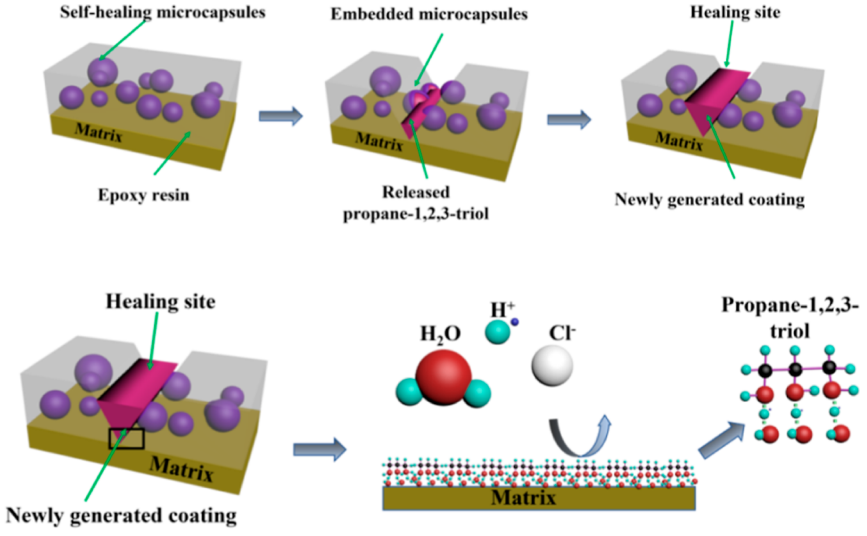

Figure 12. Schematic diagram of the self-healing mechanism.

https://doi.org/10.1021/acsomega.2c02026
ACS Omega 2022, 7, 21868−21876

friction coefficients of the self-healing coating prove that the release of the corrosion inhibitor encapsulated in the microcapsules reduces the friction coefficient of the coating.

5. In the electrochemical experiment, the microcapsules were successfully loaded into the epoxy resin coating. The corrosion inhibitor was successfully released, which was adsorbed on the corrosion site to form the corrosion inhibitor adsorption film. It reduces the corrosion of steel successfully.

■ ASSOCIATED CONTENT

Supporting Information

The Supporting Information is available free of charge at https://pubs.acs.org/doi/10.1021/acsomega.2c02026.

Photograph of synthetic procedure; SEM images of microcapsules; and Raman spectra, XRD, FTIR spectra, XPS spectra, TGA curve, EIS fitting curve, Tafel plot, and performance of corrosion resistance (PDF)

■ AUTHOR INFORMATION

Corresponding Author

Shumei Kang − *University of Science and Technology Liaoning, Anshan 114051 Liaoning, China*; Email: kangshumei_911@163.com

Authors

Qingping Zhao − *University of Science and Technology Liaoning, Anshan 114051 Liaoning, China*; orcid.org/0000-0002-5652-9822

Fangzheng Zou − *University of Science and Technology Liaoning, Anshan 114051 Liaoning, China*

Zhongbo Zhu − *University of Science and Technology Liaoning, Anshan 114051 Liaoning, China*

Jian Kang − *State Key Laboratory of Rolling and Automation, Northeastern University, Shenyang 110819 Liaoning, China*

Yansheng Yin − *Guangdong Key Laboratory of Materials and Equipment in Harsh Marine Environment, Guangzhou Maritime University, Guangzhou 510725 Guangdong, China*

Complete contact information is available at: https://pubs.acs.org/10.1021/acsomega.2c02026

Author Contributions

Data curation, F.Z. and Z.Z.; data analysis and processing, F.Z. and Q.Z.; writing original draft preparation, Q.Z.; writing review and editing, Q.Z. and S.K.

Notes

The authors declare no competing financial interest.

■ ACKNOWLEDGMENTS

The authors sincerely thank the National Natural Science Foundation of China (52074149), National Natural Fund Joint Project (U1860112), State Key Laboratory of Metal Materials for Marine Equipment and Applications Fund Joint Project [HGSKL-USTLN(2021)02], Open Program of State Key Laboratory of Rolling and Automation (2020RALKFKT008), and Open Program of State Key Laboratory of Metal Material for Marine Equipment and Application (SKLMEA-K202007).

■ REFERENCES

(1) Wang, L.; Huang, Y.; Yuan, Y.; Jia, C.; Yang, L. Microstructure, wear and oxidation resistance of Al-doped Ti−Si_3N_4 coatings by laser cladding. *Surf. Coat. Technol.* **2022**, *429*, 127942.

(2) Codescu, M. M.; Alina, V.; Victor, G.; Ionelia, V.; Iulian, P.; Mihaela, D.; Viorel, B.; Delia, P.; Mihai, I. Zn based hydroxyapatite based coatings deposited on a novel FeMoTaTiZr high entropy alloy used for bone implants. *Surf. Interfaces* **2022**, *28*, 101591.

(3) Yuan, B.; Chen, H.; Zhao, R.; Deng, X.; Chen, G.; Yang, X.; Xiao, Z.; Aurora, A.; Iulia, B. A.; Zhang, K.; Zhu, X.; Iulian, A. V.; Hai, S.; Zhang, X. Construction of a magnesium hydroxide/graphene oxide/hydroxyapatite composite coating on Mg-Ca-Zn-Ag alloy to inhibit bacterial infection and promote bone regeneration. *Bioact. Mater.* **2022**, *18*, 354−367.

(4) Yin, X.; Mu, P.; Wang, Q.; Li, J. Superhydrophobic ZIF-8 based dual-layer coating for enhanced corrosion protection of Mg alloy. *ACS Appl. Mater. Interfaces* **2020**, *12*, 35453−35463.

(5) Li, B.; Yin, X.; Xue, S.; Mu, P.; Li, J. Facile fabrication of graphene oxide and MOF-based superhydrophobic dual-layer coatings for enhanced corrosion protection on magnesium alloy. *Appl. Surf. Sci.* **2022**, *580*, 152305.

(6) Vishwakarma, A. K.; Sen Yadav, B.; Singh, J.; Sharma, S.; Kumar, N. Antibacterial activity of PANI coated $CoFe_2O_4$ nanocomposite for gram-positive and gram-negative bacterial strains. *Mater. Today Commun.* **2022**, *31*, 103229.

(7) Pham, D. Q.; Gangadoo, S.; Berndt, C. C.; Chapman, J.; Zhai, J.; Vasilev, K.; Truong, V. K.; Ang, A. S. M. Antibacterial Longevity of a Novel Gallium Liquid Metal/Hydroxyapatite Composite Coating Fabricated by Plasma Spray. *ACS Appl. Mater. Interfaces* **2022**, *14*, 18974.

(8) Xing, Q.; Zhang, S.; Gao, X.; Yu, R.; Liang, Y.; Tong, H.; Wei, S.; Fang, Y.; Wang, H.; Xiong, S. Microstructure and thermal shock resistance of Nd_2O_3 -doped YSZ-based thermal barrier coatings. *Ceram. Int.* **2020**, *46*, 26841−26853.

(9) Chen, W. L.; Wu, H. J.; Liu, M.; Xiao, X. L. Erosion Behavior of PS-PVD Thermal Barrier Coatings and the Effect of Composite Coating (PS-PVD + APS) Thickness. *Mater. Sci. Forum* **2020**, *993*, 1095−1103.

(10) Zhong, F.; He, Y.; Wang, P.; Chen, C.; Wu, Y. Novel pH-responsive self-healing anti-corrosion coating with high barrier and corrosion inhibitor loading based on reduced graphene oxide loaded zeolite imidazole framework. *Colloids Surf., A* **2022**, *642*, 128641.

(11) Sun, J.; Li, W.; Zhan, Y.; Tian, L.; Tian, H. Two preparation processes for anti-corrosion and self-healing epoxy coatings containing the poly (calcium alginate) microcapsules loaded with tung oil. *Colloids Surf., A* **2022**, *641*, 128600.

(12) Udoh, I. I.; Shi, H.; Daniel, E. F.; Li, J.; Gu, S.; Liu, F.; Han, E.-H. Active anticorrosion and self-healing coatings: a review with focus on multi-action smart coating strategies. *J. Mater. Sci. Technol.* **2022**, *116*, 224−237.

(13) Shchukina, E.; Wang, H.; Shchukin, D. G. Nanocontainer-based self-healing coatings: current progress and future perspectives. *Chem. Commun.* **2019**, *55*, 3859−3867.

(14) Panisello, C.; Peña, B.; Gumí, T.; Garcia-Valls, R. Polysulfone microcapsules with different wall morphology. *J. Appl. Polym. Sci.* **2013**, *129*, 1625−1636.

(15) Tao, Z.; Cui, J.; Qiu, H.; Yang, J.; Gao, S.; Li, J. Microcapsule/silica dual-fillers for self-healing, self-reporting and corrosion protection properties of waterborne epoxy coatings. *Prog. Org. Coat.* **2021**, *159*, 106394.

(16) Asadi, A. K.; Ebrahimi, M.; Mohseni, M. Preparation and characterisation of melamine-urea-formaldehyde microcapsules containing linseed oil in the presence of polyvinylpyrrolidone as emulsifier. *Pigm. Resin Technol.* **2017**, *46*, 318.

(17) Habib, S.; Khan, A.; Nawaz, M.; Sliem, M.; Shakoor, R.; Kahraman, R.; Abdullah, A.; Zekri, A. Self-Healing Performance of Multifunctional Polymeric Smart Coatings. *Polym* **2019**, *11*, 1519.

(18) Fadil, M.; Chauhan, D. S.; Quraishi, M. A. Smart Coating Based on Urea-Formaldehyde Microcapsules Loaded with Benzotriazole for

https://doi.org/10.1021/acsomega.2c02026
ACS Omega 2022, 7, 21868−21876

Corrosion Protection of Mild Steel in 3.5 % NaCl. *Russ. J. Appl. Chem.* **2018**, *91*, 1721−1728.
(19) Mahmoudian, M.; Nozad, E.; Kochameshki, M. G.; Enayati, M. Preparation and investigation of hybrid self-healing coatings containing linseed oil loaded nanocapsules, potassium ethyl xanthate and benzotriazole on copper surface. *Prog. Org. Coat.* **2018**, *120*, 167−178.
(20) Shahabudin, N.; Yahya, R.; Gan, S. Microcapsules Filled with a Palm Oil-Based Alkyd as Healing Agent for Epoxy Matrix. *Polym* **2016**, *8*, 125.
(21) Cordeiro Neto, A. G.; Pellanda, A. C.; de Carvalho Jorge, A. R.; Floriano, J. B.; Coelho Berton, M. A. Preparation and evaluation of corrosion resistance of a self-healing alkyd coating based on microcapsules containing Tung oil. *Prog. Org. Coat.* **2020**, *147*, 105874.
(22) Sun, J.; Li, W.; Li, N.; Zhan, Y.; Tian, L.; Wang, Y. Effect of surface modified nano-SiO_2 particles on properties of TO@CA/SR self-healing anti-corrosion composite coating. *Prog. Org. Coat.* **2022**, *164*, 106689.
(23) Khorasani, S. N.; Ataei, S.; Neisiany, R. E. Microencapsulation of a coconut oil-based alkyd resin into poly (melamine-urea-form-aldehyde) as shell for self-healing purposes. *Prog. Org. Coat.* **2017**, *111*, 99−106.
(24) Marathe, R.; Tatiya, P.; Chaudhari, A.; Lee, J.; Mahulikar, P.; Sohn, D.; Gite, V. Neem acetylated polyester polyol-Renewable source based smart PU coatings containing quinoline (corrosion inhibitor) encapsulated polyurea microcapsules for enhance anticorrosive property. *Ind. Crops Prod.* **2015**, *77*, 239−250.
(25) Qiu, L.; Zhang, M.; Adhikari, B.; Chang, L. Microencapsulation of rose essential oil in mung bean protein isolate-apricot peel pectin complex coacervates and characterization of microcapsules. *Food Hydrocolloids* **2022**, *124*, 107366.
(26) Patil, D. M.; Phalak, G. A.; Mhaske, S. T. Design and synthesis of bio-based epoxidized alkyd resin for anti-corrosive coating application. *Iran. Polym. J.* **2018**, *27*, 709−719.
(27) da Cunha, A. B. M.; Leal, D. A.; Santos, L. R. L.; Riegel-Vidotti, I. C.; Marino, C. E. B. pH-sensitive microcapsules based on biopolymers for active corrosion protection of carbon steel at different pH. *Surf. Coat. Technol.* **2020**, *402*, 126338.
(28) Li, H.; Wang, B.; Zhu, Y.; Huai, Y.; Cui, Y. Preparation and application of polysulfone microcapsules containing tung oil in self-healing and self-lubricating epoxy coating. *Colloids Surf., A* **2017**, *518*, 181−187.
(29) Li, H.; Cui, Y.; Li, Z.; Zhu, Y.; Wang, H. Fabrication of microcapsules containing dual-functional tung oil and properties suitable for self-healing and self-lubricating coatings. *Prog. Org. Coat.* **2018**, *115*, 164−171.
(30) Li, H.; Wang, Q.; Wang, H.; Cui, Y.; Zhu, Y.; Wang, B. Fabrication of Thermally Stable Polysulfone Microcapsules Containing [EMIm][NTf2] Ionic Liquid for Enhancement of In Situ Self-Lubrication Effect of Epoxy. *Macromol. Mater. Eng.* **2016**, *301*, 1473−1481.
(31) Li, H.; Wang, Q.; Li, M.; Cui, Y.; Zhu, Y.; Wang, B.; Wang, H. Preparation of high thermal stability polysulfone microcapsules containing lubricant oil and its tribological properties of epoxy composites. *J. Microencapsulation* **2016**, *33*, 286−291.
(32) Zhang, W.; Qi, X.; Li, X.; Dong, Y.; Yao, W.; Liang, L.; Zhang, Y. Surface modification of polysulfone/PAO40 microcapsules via polydopamine to improve thermal stability and used to prepare polyamide 6-based self-lubricating composite. *Colloids Surf., A* **2021**, *625*, 126906.

https://doi.org/10.1021/acsomega.2c02026
ACS Omega 2022, 7, 21868−21876